Improved Multi-DOF Haptics With Spring Drive Amplifiers

Robert P. Wilson
Telerobotics Lab
Stanford University

Günter Niemeyer
Telerobotics Lab
Stanford University

Abstract— Spring drive amplifiers utilize the natural inductive properties of a DC motor to produce stronger position feedback than is achievable with traditional current amplifiers. Impedance-type haptics devices can leverage these amplifiers to render superior contacts with higher contact stiffness. Use of these amplifiers, however, requires the virtual environment to specify motion commands for each motor.

This work extends the recently developed 1-DOF integrated approach to multi-DOF applications. It presents a motion controller working with spring drive amplifiers, together producing the maximum achievable isotropic Cartesian stiffness. Isotropy is necessary to guarantee that haptic contact forces are rendered in the correct direction. The system is implemented on a PHANTOM 1.0 haptic device and analytic performance is verified by experiment.

I. INTRODUCTION

Kinesthetic force rendering on impedance-type haptic devices is characterized by excellent free space transparency, while simulation of rigid contact remains a challenge. This issue has been explored extensively and is generally attributed to the difficulty of producing high stiffness with digital springs while maintaining stability. Energy leaks caused by non-idealities in the digitization of state measurements and force commands ultimately limit achievable stiffness gains [1], [9], [3], [4].

Motivated by the importance of high stiffness over the full bandwidth of human haptic sensitivity for clear conveyance of rigidity [8], a method of stiff motion control for haptics was recently proposed[5], [10]. It uses load-compensated voltage drives for dc motors to utilize the analog inductive stiffness as a stiff, stable haptic coupling. This motion control approach requires a quasi-static virtual environment that is completely motion-based[11].

In this paper, the controller, which we will refer to as the spring drive approach, is extended to multi-DOF devices. In particular, this generalization addresses the need for a high-level motion controller to produce haptically accurate force directions in Cartesian space. Here, the Jacobian transpose solution to the inverse kinematic problem is adopted and shown to provide a uniform stiffness in Cartesian space.

The paper begins by discussing the operation of a dc motor as a motion source through the combination of a load-compensated voltage drive and mid-level position feedback controller in Sections II and III. In Section IV the one-DOF motion control approach is reviewed before generalizing to multi-DOF in Section V. Section VI presents an experimental implementation on the PHANTOM 1.0 and concluding remarks are provided in Section VII.

II. SPRING DRIVE DESCRIPTION

In [5] the use of a voltage drive with resistive load compensation, which we will refer to as a spring drive for brevity, is shown to improve the haptic rendering of rigid contact when compared to standard current drive motor amplifiers. The key idea underlying this improvement is slowing the electrical dynamics and allowing the inductance to be utilized as a high-stiffness haptic coupling. This concept and the corresponding notation are covered briefly in this section.

The electrical dynamics of a typical brushed dc motor are

$$e_A(t) = Ri(t) + L\frac{di(t)}{dt} + e_B(t) \tag{1}$$

with coupling equations

$$e_B(t) = k_T\dot{\theta}(t) \tag{2}$$
$$\tau(t) = k_T i(t), \tag{3}$$

where e_A is the applied voltage, e_B is the back-EMF, k_T is the torque/speed constant, τ is the motor torque, i is the winding current, $\dot{\theta}$ is the rotor velocity, and R and L are the winding resistance and inductance, respectively. In order to pursue a haptic perspective on the effects of driving a motor with the spring drive, it is useful to interpret R and L as an equivalent mechanical spring K_L

$$K_L = \frac{k_T^2}{L} \tag{4}$$

and damper B_R,

$$B_R = \frac{k_T^2}{R}, \tag{5}$$

where K_L and B_R are connected in series. The spring drive approach couples the haptic device to the virtual environment through K_L, which is available at all frequencies, inherently stable, and very stiff for small L. It proposes to lock and eliminate B_R by canceling the winding resistance.

Resistance cancellation is accomplished by setting

$$e_A = \hat{R}i + e_W \tag{6}$$

which effectively cancels the voltage drop across the winding resistance, while allowing additional voltage inputs e_W. Implementation of (6) is accomplished by closing a positive current feedback loop with gain $\hat{R}$ around a voltage drive in analog circuitry.

e-mail: rpwilson@stanford.edu
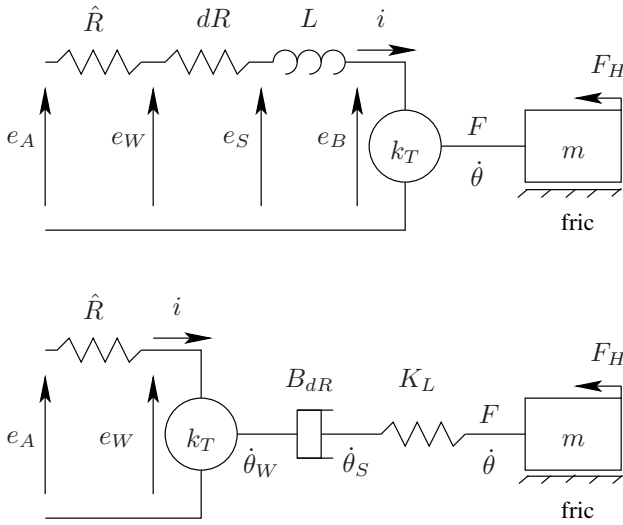e-mail: gunter.niemeyer@stanford.edu

Fig. 1. MOTOR INDUCTANCE AND RESIDUAL RESISTANCE ARE MAPPED FROM THE ELECTRICAL DOMAIN TO THE MECHANICAL DOMAIN

Since the motor resistance R varies with temperature and brush commutation, a residual uncanceled resistance

$$dR(T,\theta) = R(T,\theta) - \hat{R}, \qquad (7)$$

will remain. It corresponds to the residual series damper

$$B_{dR} = \frac{k_T^2}{dR}. \qquad (8)$$

Fig. 1 shows the mapping of winding inductance L and residual resistance dR into the mechanical domain, leaving $\hat{R}$ to be canceled by (6). By the electromechanical coupling (2), the intermediate voltages e_W and e_S relate to the velocities $\dot{\theta}_W$ and $\dot{\theta}_S$, respectively; where e_W is the applied node voltage between the series resistances $\hat{R}$ and dR, e_S is the node voltage between R and L, $\dot{\theta}_W$ is the velocity of the setpoint of the mechanical equivalent series spring-damper, and $\dot{\theta}_S$ is the velocity of the connection point between the series spring and damper. With the inductance and residual resistance interpreted in the physical domain, voltage commands to the spring drive are equivalent to velocity commands to the set-point of the series spring-residual damper

$$e_W = k_T \dot{\theta}_W. \qquad (9)$$

Therefore, the spring drive operates the dc motor as an approximate motion source. This is in contrast with the current drive motor amplifiers typically used in haptic devices, which speed up the electrical dynamics and operate the motor as a torque source. By recasting the motor as a motion source, it becomes necessary to design the digital controller as a motion controller, again in contrast to the impedance control typically paired with the current drive.

III. MID-LEVEL DRIFT COMPENSATION

Before any high-level controller can be successfully implemented, the fact that a residual damper B_{dR} exists between the commanded location θ_W and the output must be

addressed. Without compensation, B_{dR} will allow θ_S and θ to drift unboundedly under low frequency external loads. In haptic applications this drift will degrade the simulation by making sustained rigid contacts feel like dampers. Therefore, position feedback with PD compensation is added digitally to combat drift and yields the control law

$$e_W = k_T \dot{\theta}_{S_d} + K_D(\dot{\theta}_{S_d} - \dot{\theta}) + K_P(\theta_{S_d} - \theta), \qquad (10)$$

where K_P and K_D are the error gains. We assume a first order filter with cutoff frequency λ on the differentiated velocity signal $\dot{\theta}$. This constitutes a mid-level controller interface between the analog inductive stiffness of the spring drive and the high-level motion controller described in the next section.

Implementation of this mid-level controller establishes a hybrid coupling between the user and the virtual environment consisting of the physical motor dynamics, analog electronics modifying those dynamics, and digital drift compensation. The combined physical and analog components comprise the series spring-damper shown in Fig. 1, while the digital component connects the parallel spring-damper of (10) between θ and θ_{Sd}. Functionally, the analog stiffness K_L dominates for high frequency deflections, while the digital mid-level controller provides low to mid frequency stiffness. The frequency-dependent stiffness transfer function for the complete coupling is found by substituting (10) into the resistance-canceled motor dynamics

$$e_W(t) = dRi(t) + L\frac{\mathrm{d}i(t)}{\mathrm{d}t} + e_B(t) \qquad (11)$$

and is

$$K_\theta(s) = \frac{\tau}{\theta}(s) = -\frac{k_T}{Ls + dR}\frac{\lambda}{s + \lambda}$$
$$\left[\left((k_T + K_D + \frac{K_P}{\lambda})s + K_P \right) + \frac{k_T s^2}{\lambda} \right]. \qquad (12)$$

For a detailed derivation and analysis of this result, see [11].

The magnitude Bode plot of (12) shown in Fig. 2 illustrates the combination of several factors that shape stiffness over frequency. Starting from the natural motor dynamics represented by the dotted curve, the spring drive lowers the corner frequency from R/L to dR/L. The proportional term in the mid-level controller then pulls the low frequency rolloff caused by B_{dR} up to a dc stiffness

$$K_{DC} = \frac{k_T K_P}{dR}, \qquad (13)$$

while the derivative term boots stiffness at midrange frequencies before the filter rolls it off to the high frequency stiffness

$$K_{HF} = K_L = \frac{k_T^2}{L}. \qquad (14)$$

While not discussed here in detail it is worth noting that, K_L may be increased by electrically reducing L in addition to R. This can be accomplished by replacing the positive feedback gain $\hat{R}$ in (6) with lead compensation as described in [6].
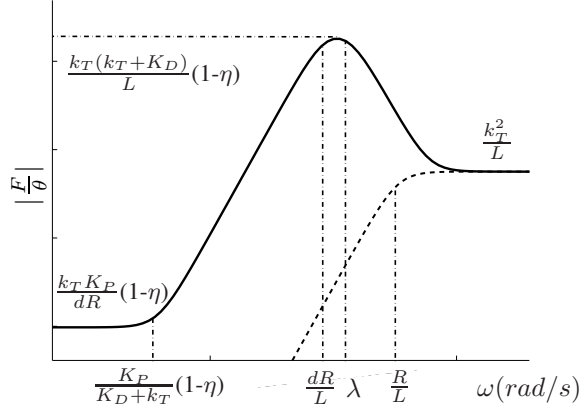
Fig. 2. FREQUENCY-DEPENDANT RENDERED STIFFNESS OF THE COMBINED SPRING DRIVE AND CONTROLLER. THE UNMODIFIED MOTOR DYNAMICS (DOTTED CURVE) ARE INCLUDED FOR COMPARISON

Thus, for a given motor the spring drive approach calls for the robustly stable minimization of dR and maximization of K_P and K_D in order to achieve the highest possible maximum stiffness at all frequencies. This tuning is then locked in place and the resulting $K_\theta(s)$ is treated as a passive coupling between the rotor angle θ and the setpoint θ_{S_d}. This $K_\theta(s)$, which we will refer to as the coupling stiffness, represents the stiffest contact that the virtual environment can render on this actuator.

IV. MOTION CONTROL OF HAPTIC DEVICES: ONE-DOF

By treating the spring driven dc motor and the mid-level drift compensator as a black-boxed motion source that accepts setpoint motion commands θ_{Sd} and $\dot{\theta}_{Sd}$, we now describe a high-level motion controller in the form of a quasi-static virtual environment (VE). Originally proposed for a single degree of freedom (DOF) in [11], this approach combines the excellent free-space performance of an impedance-type device with the improved contact performance of an admittance-like controller. The structure of this VE is developed here for the one-DOF case before generalization to multiple degrees of freedom in the next section.

As described in Section III, θ_{Sd} and $\dot{\theta}_{Sd}$ command the setpoint of the coupling stiffness $K_\theta(s)$. Thus, it is sufficient for the haptic simulation to implement a very simple, purely motion-based VE that uses a virtual proxy or tool to determine θ_{Sd}, effectively using the coupling stiffness as the connection between the user and the VE. Rigid contact is easily rendered by commanding zero motion and locking the coupling stiffness

$$\dot{\theta}_{S_d} = 0 \qquad \theta_{S_d} = \theta_0, \qquad (15)$$

where θ_0 is the location of the contact constraint.

Freespace is accomplished by setting the desired motion to track the user

$$\dot{\theta}_{S_d} = \dot{\theta} \qquad \theta_{S_d} = \theta. \qquad (16)$$

A slight lag in filtering the velocity may cause the system to create slight non-zero forces, equivalent to an added mass. Given the low bandwidth of human actions compared to the speed of filtering, however, any added mass tends to fall far below perceptible levels.

Finally, compliant contact is achieved by setting the desired motion to a fraction of the user motion. The full dynamic range of the VE can be represented by

$$\dot{\theta}_{S_d} = \eta\dot{\theta} \qquad \theta_{S_d} = \eta\theta + (1-\eta)\theta_0, \qquad (17)$$

where $0 \leq \eta \leq 1$, and $\eta = 0$ and $\eta = 1$ correspond to rigid contact and freespace, respectively. The low-frequency output stiffness is reduced by the factor η.

As a motion-based VE, no absolute force values are available, either explicitly via measurement or implicitly by commanding motor current. Output stiffnesses, therefore, may no longer be programmed exactly, but must be specified as a fraction of the device's maximum achievable stiffness. Knowledge of $K_\theta(s)$, particularly K_{DC}, can be used to estimate values. Additional discussion of this high-level controller may be found in [11].

V. MOTION CONTROL OF HAPTIC DEVICES: MULTI-DOF

In extending the above approach to multi-DOF haptics, we recognize the application's requirements. Though we wish to display the maximum achievable stiffness, force directions need to be rendered accurately to convey proper geometric surface properties. For example, forces should always fall perpendicular to frictionless surfaces. To support this requirement, perceived output stiffnesses need to be spatially uniform.

Given an n-DOF device, one drift-compensated spring drive is used to drive each joint motor. Thus, each joint independently replicates the one-DOF system described in Section III, acting as a joint motion source with a stiffness described by (12). We assume here that all joints exhibit the same stiffness, though relative scaling between joints could be incorporated if necessary. We define a desired Cartesian location $\vec{x}_{Sd}$ and velocity $\dot{\vec{x}}_{Sd}$, and collect the individual joint values into a joint position vector $\vec{q}$ and velocity vector $\dot{\vec{q}}$ with equivalent desired position $\vec{q}_{Sd}$ and velocity $\dot{\vec{q}}_{Sd}$,

$$\vec{q}_{Sd} = invkin(\vec{x}_{Sd}) \qquad \dot{\vec{q}}_{Sd} = \mathbf{J}^{-1}\dot{\vec{x}}_{Sd} \qquad (18)$$

obtained by inverting the mechanism's kinematics. This will produce joint torques

$$\vec{\tau} = \mathbf{K_q}\Delta\vec{q} \qquad (19)$$

via a diagonal joint stiffness matrix

$$\mathbf{K_q} = K_\theta(s)\mathbf{I}, \qquad (20)$$

which maps to a Cartesian stiffness of

$$\mathbf{K_x}^{\mathbf{inv}} = \mathbf{J^{-T}K_qJ^{-1}} = K_\theta(s)(\mathbf{JJ^T})^{-1} \qquad (21)$$

remembering that

$$\vec{F} = \mathbf{K_x}^{\mathbf{inv}}\Delta\vec{x} \qquad \vec{\tau} = \mathbf{J^T}\vec{F} \qquad \Delta\vec{x} \approx \mathbf{J}\Delta\vec{q}. \qquad (22)$$

We denote the stiffness matrix with 'inv' to indicate the joint values were set by an inverse Jacobian kinematic algorithm.

Unfortunately, this Cartesian stiffness is non-spherical such that forces are not necessarily generated along displacement vectors. Fig. 3 depicts such a stiffness ellipsoid for a simple 2-DOF case. Proper haptic rendering of force requires that the multi-DOF motion controller reshape this ellipsoid into a sphere.

We instead propose to calculate

$$\vec{q}_{Sd} = \vec{q} + \alpha \mathbf{J^T}(\vec{x}_{Sd} - \vec{x}) \qquad (23)$$

and approximate the set-point derivative as

$$\dot{\vec{q}}_{Sd} = \dot{\vec{q}} + \alpha \mathbf{J^T}(\dot{\vec{x}}_{Sd} - \dot{\vec{x}}), \qquad (24)$$

where we ignore the Jacobian's derivative. By construction this simplification only affects forces rendered at high velocities and high frequencies with minimal impact on user perception as discussed at the end of this section. This delivers a Cartesian force $\vec{F}$ of

$$\vec{F} = \mathbf{J^{-T}K_q}\alpha \mathbf{J^T}\Delta\vec{x} \qquad (25)$$

and the Cartesian stiffness

$$\mathbf{K_x^{trans}} = \alpha \mathbf{J^{-T}K_q J^T}. \qquad (26)$$

Since $\mathbf{K_q}$ is the scaled identity matrix, $\mathbf{K_x^{trans}}$ collapses to the diagonal

$$\mathbf{K_x^{trans}} = \alpha K_\theta(s)\mathbf{I}. \qquad (27)$$

Effectively, the transpose algorithm (23) has reshaped the ellipsoid into a sphere and restored the force directions to parallel any deflections.

Having resolved the force direction problem, there is now the issue of what value to select for α. To address this, first recall that each joint is tuned for a maximum joint stiffness $K_\theta(s)$. Also note that locking each joint results in the Cartesian stiffness $\mathbf{K_x^{inv}}$. Thus, $\mathbf{K_x^{inv}}$ represents the maximum achievable Cartesian stiffness for a given configuration, limited by the stability of each joint. Using the Jacobian transpose solution to the inverse kinematics has reshaped $\mathbf{K_x^{inv}}$ into the Cartesian stiffness ball $\mathbf{K_x^{trans}}$, which must now be appropriately scaled by α. Intuitively, $\mathbf{K_x^{trans}}$ cannot be scaled arbitrarily large, as this would allow the effective Cartesian stiffness to be increased without bound. Indeed, if the magnitude of $\mathbf{K_x^{trans}}$ exceeds that of $\mathbf{K_x^{inv}}$ in any direction, we would be asking for a stiffness beyond the stable maximum. Doing this would effectively increase the gains of one or more joint controllers and compromise their stability. Therefore, taking $\mathbf{K_x^{inv}}$ as the upper bound to maintain stability, the eigenvalues of $\mathbf{K_x^{trans}}$ must satisfy

$$\lambda_{max}(\mathbf{K_x^{trans}}) \leq \lambda_{min}(\mathbf{K_x^{inv}}). \qquad (28)$$

Substituting (27) and (21), this condition simplifies to

$$\alpha \leq \lambda_{min}[(\mathbf{JJ^T})^{-1}], \qquad (29)$$

where $\lambda_{min}[(\mathbf{JJ^T})^{-1}]$ may be computed on the fly to maximize $\mathbf{K_x^{trans}}$ independently for each configuration, or
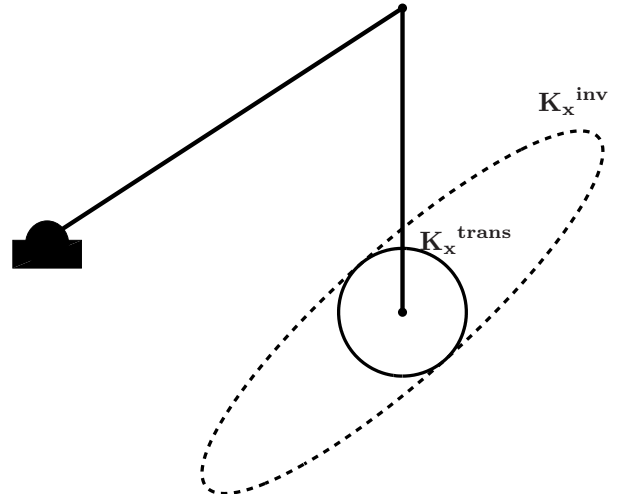

Fig. 3. CARTESIAN STIFFNESS ELLIPSES $\mathbf{K_x^{inv}}$ AND $\mathbf{K_x^{trans}}$ WITH $\alpha = \lambda_{min}[(\mathbf{JJ^T})^{-1}]$ FOR A 2-DOF MANIPULATOR (PHANTOM WITH LOCKED BASE JOINT).

computed over the entire workspace offline to select the global minimum for a consistent $\mathbf{K_x^{trans}}$ at all configurations.

Fig. 3 illustrates the ellipses $\mathbf{K_x^{inv}}$ and $\mathbf{K_x^{trans}}$ with $\alpha = \lambda_{min}[(\mathbf{JJ^T})^{-1}]$ for a PHANTOM constrained to 2-DOF by locking its base motor. This configuration will be revisited experimentally in the next section.

The stiffness shape compensation performed by this mult-DOF VE does not have infinite bandwidth. As a result $\mathbf{K_x^{inv}}$ will still exist at high frequencies, and impulsive force vectors may be directed incorrectly. Since these direction discrepancies exist only at high frequency, however, the user will likely be unable to detect them kinesthetically, due to a low perceptual bandwidth of $20Hz$ to $30Hz$ [7]. Tactile detection of the discrepancy may fare better, but [2] indicates that the direction discrimination threshold is only about $25°$, determined for perception of low frequency forces. Informal experience with a multi-DOF implementation on a PHANTOM 1.0 suggests that these discrepancies are not perceptible, and certainly not disruptive to the haptic simulation, however, further investigation of human sensitively to impulse force direction may be interesting.

Similar to the one-DOF case, compliant surfaces and free space may be obtained by setting

$$\dot{\vec{x}}_{Sd} = \eta\dot{\vec{x}} \qquad \vec{x}_{Sd} = \eta\vec{x} + (1-\eta)\vec{x}_0, \qquad (30)$$

with $0 \leq \eta \leq 1$.

VI. EXPERIMENTAL IMPLEMENTATION

The multi-dof motion control approach described above was implemented on a PHANTOM 1.0 haptic device in order to confirm the generation of correct force vectors.

Evaluation of force direction was accomplished by mounting a six-axis force sensor to the end effector of the PHANTOM and then fixing both the PHANTOM base and the sen-

Fig. 4. EXPERIMENTAL SETUP: BOTH THE PHANTOM AND FORCE SENSOR ARE FIXED TO THE TABLE. THE DIRECTION OF STATIC FORCES IS MEASURED.

Fig. 5. 2-DOF FORCE VECTORS PRODUCED BY DIFFERENT IN-VERSE KINEMATIC SOLUTIONS. THE CORRECT REACTION FORCE FOR PENETRATION OF THE VIRTUAL WALL IS SHOWN BY THE DOTTED LINE.

sor to ground. This effectively locked the PHANTOM into a fixed configuration, holding all configuration-dependent variables constant. Fig. 4 is a photo of the setup, which features the same configuration as shown in Fig. 3. With the PHANTOM locked, virtual surfaces were then specified so that the device was already in a penetration state and the resulting force direction was recorded.

The results in Fig. 5 compare the realized reaction forces under both the Jacobian inverse and proposed Jacobian transpose control for a horizontal wall placed above the device. Here, the device is represented by the black circle, and the dotted line indicates the correct reaction force vector. As expected, the Jacobian transpose produces an accurately directed force while Jacobian inverse control exhibits significant deviation.

Fig. 6 reflects the results of repeating this experiment for additional virtual surfaces. These surfaces are specified tangentially around the unit circle in the 2-D plane of Fig. 5 with a radial spacing of $15°$. The plot displays the angular error between the measured and correct force directions in each case. As expected, Jacobian transpose control provides low errors. Additionally, it is not well correlated with the angle of the surface normal, which suggests the corresponding Cartesian stiffness is circular. Jacobian inverse control, on the other hand, produces large errors that are strongly and periodically correlated with the normal direction, indicative of an elliptical Cartesian stiffness.

VII. CONCLUSION

Generalization of one-DOF motion control of impedance-type haptic devices to multiple degrees of freedom is achieved through the use of Jacobian transpose control. The system acts to regulate the Cartesian stiffness to a uniform
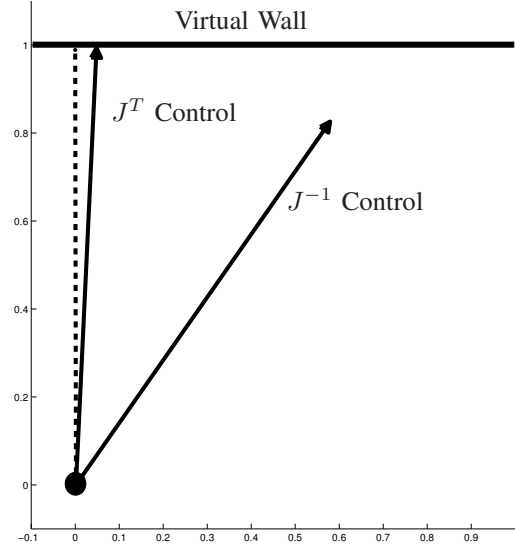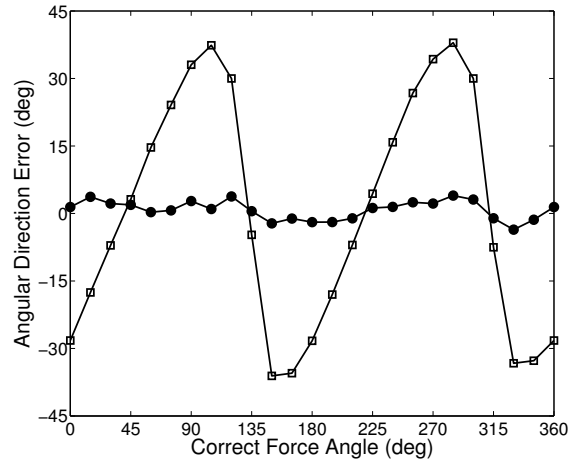

Fig. 6. ANGULAR FORCE DIRECTION ERROR OF $\mathbf{J^T}$ CONTROL (●) AND $\mathbf{J^{-1}}$ CONTROL (□). THE PERIODIC ERROR OF $\mathbf{J^{-1}}$ CON-TROL RELECTS THE CORRESPONDING ELLIPTICAL CARTESIAN STIFFNESS

sphere. The resulting haptic simulation produces accurately directed force vectors in response to motion constraints, while taking advantage of the high analog stiffness of load-compensated voltage motor drivers.

This spring drive approach contrasts with traditional haptic impedance control by setting a maximum stiffness in the low-level actuator and using high-level control to scale the rendered stiffness between freespace and this maximum. While the loss of force calculations in the virtual environment prevents the coding of absolute virtual stiffnesses, this limitation is traded off by the improved perceptual performance.

We hope extending the spring drive's superior performance

to a commercial multi-DOF haptic device will enhance future haptic applications and improve the user's experiences.

VIII. ACKNOWLEDGMENTS

REFERENCES

[1] J. Abbott and A. Okamura, "Effects of position quantization and sampling rate on virtual-wall passivity," *IEEE Transactions on Robotics*, vol. 21, no. 5, pp. 952–964, Oct. 2005.

[2] F. Barbagli, K. Salisbury, C. Ho, C. Spence, and H. Z. Tan, "Haptic discrimination of force direction and the influence of visual information," *ACM Trans. Appl. Percept.*, vol. 3, no. 2, pp. 125–135, 1 06.

[3] J. E. Colgate and G. Schenkel, "Passivity of a class of sampled-data systems: Application to haptic interfaces," in *Proceedings, American Control Conferences, Baltimore, Maryland*, vol. 3, June/July 1994, pp. 3236–3240.

[4] N. Diolaiti, G. Niemeyer, F. Barbagli, and J. Salisbury, J.K., "Stability of haptic rendering: Discretization, quantization, time delay, and coulomb effects," *IEEE Transactions on Robotics*, vol. 22, no. 2, pp. 256–268, April 2006.

[5] N. Diolaiti, G. Niemeyer, and N. A. Tanner, "Wave Haptics: Building Stiff Controllers from the Natural Motor Dynamics," *The International Journal of Robotics Research*, vol. 26, no. 1, pp. 5–21, 2007.

[6] R. Gorez and J. O'shea, "Robots positioning control revisited," *Journal of Intelligent and Robotic Systems*, vol. 3, no. 3, pp. 213–231, Sept 1990.

[7] K. Hale and K. Stanney, "Deriving haptic design guidelines from human physiological, psychophysical, and neurological foundations," *IEEE Computer Graphics and Applications*, vol. 24, no. 2, pp. 33–39, March-April 2004.

[8] D. Lawrence, L. Pao, A. Dougherty, M. Salada, and Y. Pavlou, "Rate-hardness: a new performance metric for haptic interfaces," *IEEE Transactions on Robotics and Automation*, vol. 16, no. 4, pp. 357–371, Aug 2000.

[9] M. Mahvash and V. Hayward, "High-fidelity passive force-reflecting virtual environments," *IEEE Transactions on Robotics*, vol. 21, no. 1, pp. 38–46, Feb. 2005.

[10] R. Wilson and G. Niemeyer, "Exploiting inate motor dynamics for high stiffness haptic display on brushless dc motors," in *Proceedings of the ASME Dynamic Systems and Controls Conference, Ann Arbor, Michigan*, Oct 2008.

[11] ——, "Motion control of impedance-type haptic devices," in *Proceedings of the IEEE International Conference on Robotics and Automation, Kobe, Japan*, May 2009.